



ELECTRODISSOLUTION AND CORROSION OF CuInS_2 PHOTOANODES WITH LAMELLAR MORPHOLOGY

S. CATTARIN,* P. GUERRIERO,† N. DIETZ‡§ and H. J. LEWERENZ‡

*Istituto di Polarografia ed Electrochimica Preparativa del C. N. R., Corso Stati Uniti 4, 35100 Padova, Italy

†Istituto di Chimica e Tecnologia dei Radioelementi del C. N. R., Corso Stati Uniti 4, 35100 Padova, Italy

‡Hahn-Meitner-Institut, Bereich Photochemische Energieumwandlung, Glienicker Strasse 100, 14109 Berlin, Germany

(Received 27 September 1993; in revised form 10 December 1993)

Abstract—Crystals of $n\text{-CuInS}_2$ grown in a steep temperature gradient show lamellar morphology, prone to cleavage, and inclusions of copper-poor phases like CuIn_2S_6 . Photoelectrooxidation of $n\text{-CuInS}_2$ in 1 M HClO_4 , a non-protective electrolyte, results in massive dissolution of the metal ions and deposition of sulfur, with marked photocurrent quenching. Operation of $n\text{-CuInS}_2$ (photo)anodes in acidic polyiodide medium causes significant corrosion and decay of photocurrent output. Micrographs of corroded areas show progressive and irregular etching of the CuInS_2 layers, which appear strongly polycrystalline. EDX microanalyses show very similar composition before and after corrosion, suggesting that the latter causes stoichiometric removal and dissolution of the components and does not form new phases of significant thickness.

Key words: CuInS_2 , photoanodes, corrosion, electrodi dissolution.

INTRODUCTION

The performance of solar cells depends in a critical way on the properties of the thin interface layer where charge generation and separation occur. The achievement of junction stability is a fundamental requisite of any device aiming at practical application and this is especially true for photoelectrochemical cells in which semiconductor (photo)corrosion is largely the rule, as predicted by thermodynamics[1, 2] and confirmed in most cases. However, (photo)corrosion may also be used to perform controlled modifications of the surface of semiconducting samples[3, 4], or to remove progressively surface layers when interest lies in characterizing the depth profile of certain material properties.

CuInX_2 photoanodes normally undergo corrosion processes in polyiodide solutions[5, 6]. Surface analyses of CuInSe_2 , by far the most widely investigated, show the presence of InI_3 and strong copper depletion[6]. The stability of CuInSe_2 in polyiodide may be substantially improved by the formation of a protective interface film either *ex situ*, prior to operation[6] or *in situ*, provided that the solution is properly modified[7].

We report elsewhere the good performance of $n\text{-CuInS}_2$ photoanodes prepared by a novel method[8], for which maximum photoconversion efficiencies of about 7% were observed. The chal-

copyrite crystal is grown in a steep temperature gradient and thereby acquires a kind of lamellar structure[9, 10], similar to that of layered compounds (eg WSe_2), which allows preparation of very thin electrodes and thus reduces the series resistance of the photocell. In this paper we investigate the processes of oxidative decomposition, both in a non-protecting electrolyte and in the polyiodide solution, with the aim of better characterizing the stability of photocells and other aspects of the corrosion processes peculiar to lamellar morphology.

EXPERIMENTAL

The CuInS_2 material was part of an ingot prepared with the gradient freeze technique at the Hahn Meitner Institut[9, 10]. Crystal sections for SEM investigations were prepared by means of a cutter, to avoid damage or formation of powdery deposits during sawing and lapping. To prepare electrodes, ingot slices were sawn into rectangular pieces, which were cleaned in boiling chloroform and methanol, back-contacted by evaporating a 100 nm thick indium layer and fixed with silver epoxy to brass holders. The crystal thickness was then decreased down to values in the range 30–100 μm (as estimated from microscope inspection and SEM pictures) by repeatedly peeling off crystal layers with adhesive tape. After encapsulation in epoxy resin (Scotchcast 3M 10/XR 5241) the electrodes had geometric surfaces in the range 4–10 mm^2 .

Solutions were prepared from water deionized and

§ Present address: Department of Materials Science and Engineering, North Carolina State University, Raleigh, NC 27695-7919 U.S.A.

purified by a Millipore Milli-RO system, and analytical grade chemicals (Merck or Carlo Erba), used without further purification. Deaerated 1 M HClO₄ was used for photoelectrodissolution experiments. The polyiodide solution consisted of 2.5 M CaI₂, 2 M HI and 40 mM I₂ and was used in contact with the air; its potential was 0.10 ± 0.01 V vs. *sce*. A mixture of H₂O/H₂O₂/H₂SO₄ 2/1/1 was used to perform chemical etching treatments. Experiments were performed in a two-compartment glass cell equipped with an optical flat on the side; working and counter electrodes were inserted in the same compartment, the *sce* reference in a side arm connected to the main compartment by a Luggin capillary. All potentials, unless otherwise indicated, are accordingly referred to the *sce*.

A common setup was used for photoelectrochemical experiments: a 100 W tungsten halogen lamp; monochromator (Applied Photophysics); filters (Schott); light chopper (EG&G Brookdeal Model 9479); potentiostat and function generator (Amel Mod. 553 and Mod. 568, respectively). Monochromatic light power was measured with a calibrated photodiode (Macam Photometrics). White light power was measured with a wide-band pyroelectric radiometer (Laser Precision Corporation, RKP-575 probe and RK-5710 readout). Recordings were taken on a Philips PM 8272 recorder.

SEM micrographs were taken using a Philips XL 40 LaB₆ apparatus, equipped with a secondary electron detector (SE) and a solid state detector for back-scattered electrons (BSE). Quantitative standardless microanalyses were obtained using an EDX PV 99 X-ray spectrometer equipped with a thin Be window. ZAF corrections were made to quantitative measurements, taken with an accelerating voltage of 25 keV. A windowless arrangement and a lower voltage (5 keV) were used for qualitative assessment of oxygen on the surface of corroded electrodes.

RESULTS AND DISCUSSION

Crystal structure and morphology

The material has a lamellar aspect, shown in Fig. 1a by the SEM micrograph of a crystal section. Cleavage occurs easily on (112) planes[9], forming an angle of about 39° with the freezing direction[10]. Micrographs taken at high magnification show that the layers have variable thickness, between a few tenths of μm and a few μm ; each layer is formed of densely packed, filamentous microcrystals (Fig. 1b), forming an estimated angle of 55° with the cleavage plane, corresponding to the angle between (112) plane and [110] direction in the chalcopyrite structure. Figure 1b suggests that the microstructure of the layer may be compact (bottom part) or partially empty, with a kind of tubular morphology (upper part).

SEM micrographs show on the cleavage surface darker and brighter regions (Figs 1a, and 2), the latter corresponding to copper-poor phases. Figure 2, top, shows the micrograph of a heterogeneous area, on which microanalyses were taken along the indicated line of xs, giving the compositions reported

in Fig. 2, bottom. It appears that the composition closely corresponds to CuIn₃S₂ in the darker area and to CuIn₃S₅ in the brighter area. The latter stoichiometry might well result from partial contribution to the signal of CuIn₃S₈ and CuInS₂ phases, which are the best known for the Cu/In/S system and show the largest signals in X-ray diffractograms[10]. However, evidence of a CuIn₃X₅ phase has been reported in the literature for X = Se[11]; the phase was identified as an ordered vacancy compound, with ordered Cu vacancies and an ordered exchange of Cu with In. More recently, stoichiometries close to 1/3/5 have been observed during XPS investigations of the surface of evaporated CuInS₂ films[12]. Hence, the frequent presence on the cleavage planes of lamellar material of Cu/In/S stoichiometries close to 1/3/5 may tentatively be attributed to formation of a distinct CuIn₃S₅ phase.

Macroscopic copper-poor phases are seldom observed in sections like that of Fig. 1b, and are seen more frequently on the surfaces obtained by peeling off the crystal sheets. Whereas this may be partially attributed to the more favourable conditions of inspection in the latter case, it may also result from a preferential crystal cleavage near and possibly due to these foreign phases. This fact may also partially explain the results of previous XPS investigations, indicating large deviations of the [Cu]/[In] ratio from the nominal stoichiometry on the surface of crystals cleaved in vacuum[9].

Cyclic voltammetry in HClO₄

Dissolution behaviour was investigated in an acidic non stabilizing electrolyte (1 M HClO₄), in pH conditions similar to those of the polyiodide solution. Figure 3 reports the cyclic voltammograms recorded in the dark (broken line) and under illumination with light of 750 nm (full line), using an electrode with homogeneous CuInS₂ composition as estimated by EDX.

At the fresh electrode, in the negative potential region little cathodic current is observed up to the limit of -1.0 V (Fig. 3a, first cycle), indicating little hydrogen evolution at a non-catalytic surface. On sweeping the potential in a positive direction, the dissolution rate is limited in the dark by carrier supply and remains very low under reverse bias up to the explored potential limit of 0.5 V. Performing the voltammetric scans under illumination, anodic photocurrent appears at potentials positive of -0.65 V and remains low up to about 0.0 V, with a kind of sluggish "prewave". The potential of photocurrent onset is about 100 mV more positive than that observed in acidic polyiodide solution (see Fig. 7), in which the flatband potential was estimated at -0.77 ± 0.05 V[8]. The quantum yield for the photodissolution process remains below 0.03 (electrons in the circuit per incident photon) up to about 0 V. It increases quite steeply on sweeping the potential further in a positive direction and reaches typical values in the range 0.35–0.45 at 0.5 V, with a subsequent tendency to saturation. Upon reversing the sweep, little hysteresis is observed in the voltammetric profile until 0 V, when the photocurrent



Fig. 1. SEM micrographs illustrating layered structure of material at two different magnifications (see bar). Note in side view (b) fine structure of layers, with microcrystals forming an angle of about 55° with cleavage plane.

appears to be quenched; below -0.1 V the total current becomes negative, showing a reduction pattern with little structure up to the limit of -1.0 V.

During the first five cycles (with a typical oxidation charge of about 20 mC cm^{-2} in each cycle), little variation in voltammetric profile is observed in the positive potential limit. At the negative limit a progressive increase in the current is observed upon cycling (Fig. 3b, cycle 5), which is mainly accounted for by increased hydrogen evolution. This modification may be due to the formation of metallic islands upon reduction of metal ions generated during anodization.

Photoelectrodissolution

By polarizing the electrode at 0.4 V vs. *sce* in 1 M HClO_4 and illuminating with monochromatic light at 750 nm (power of about 2.5 mW cm^{-2}), a steady

oxidation current without significant transients is observed. The SEM pictures of the corroded surface (Fig. 4) show that dissolution is concentrated in corrosion pits, both deep and shallow, quite homogeneously distributed, and with a triangular shape similar to that observed on CuInSe_2 (112) surfaces[13]. Current density, originally in the range 0.5 – 0.6 mA cm^{-2} , decreases by only 10–20% over a period of 10 min, during which time a charge of about 300 mC cm^{-2} is passed, corresponding to formal oxidation of hundreds of monolayers. On increasing the oxidation charge, the surface becomes quite homogeneously pitted with deep triangular cavities, progressively merging. Microanalysis of material in the pits shows small increases in the sulfur content and in the copper to indium ratio, suggesting that during the early stages of (photo)electro-oxidation the products largely dis-

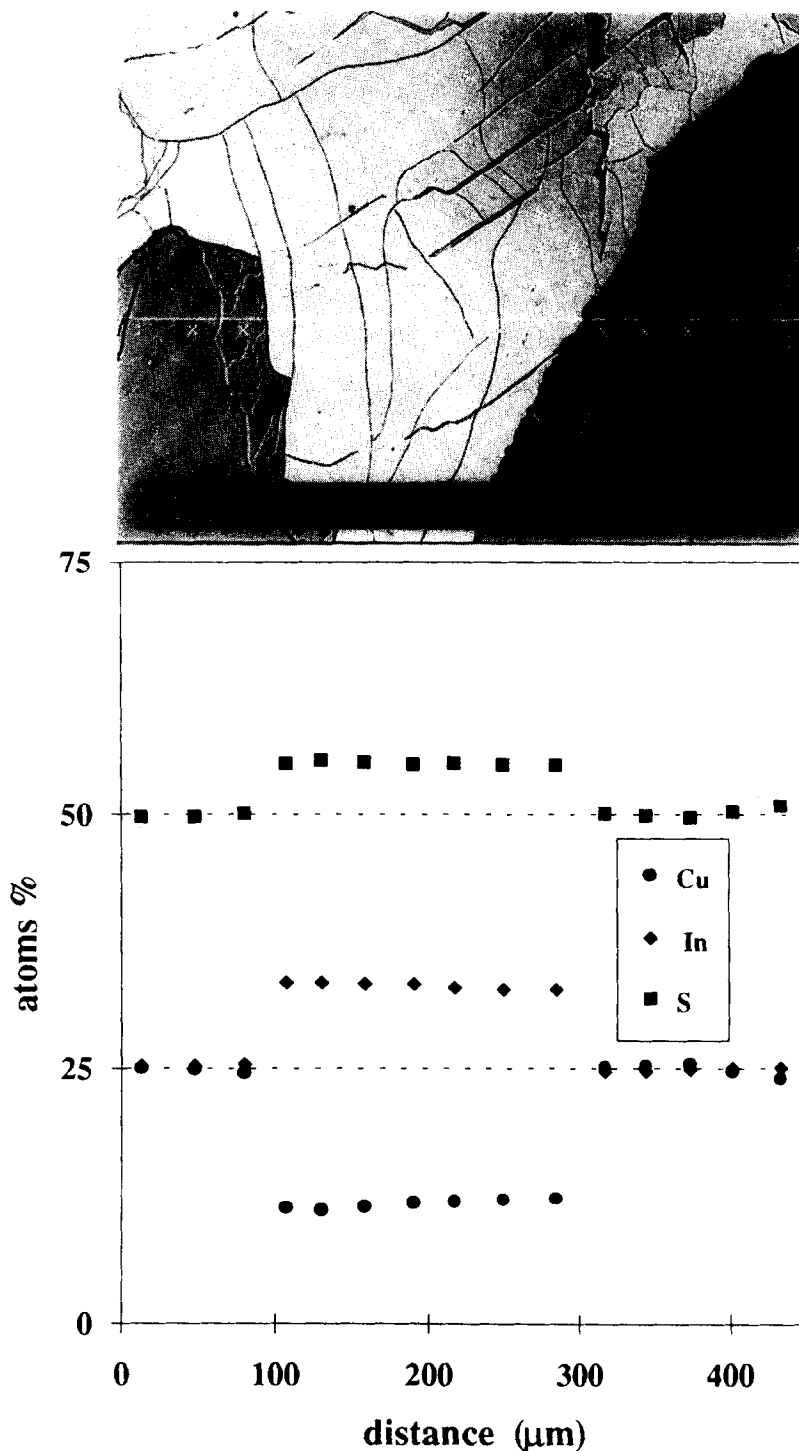


Fig. 2. SEM micrograph (top) of a crystal with different Cu/In/S phases on surface and relevant composition profile obtained by EDX (bottom). Stoichiometry varies sharply from CuInS_2 (darker area) to CuIn_3S_5 (brighter area).

solve, the metals as cations and the chalcogen either as elemental sulfur or as soluble oxygenated species, with resulting limited photocurrent quenching.

Massive electrodisolution was performed by polarizing the electrode at 0.4 V under white light and regulating the photon flux so as to obtain an initial current density of about 20 mA cm^{-2} . Current evolution depends significantly on the sample, but

the pattern is qualitatively reproducible (Fig. 5): early on, there is a short period of fairly constant current, sometimes with a temporary increase, then a quite steep decrease after which the current reaches a low value and decreases further more slowly. An integrated oxidation charge of $3\text{--}5 \text{ C cm}^{-2}$ was passed in typical experiments.

The effect of massive electrodisolution is illus-

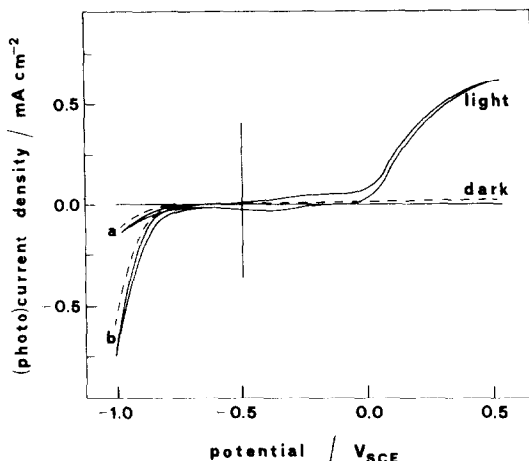


Fig. 3. Cyclic voltammograms recorded in deaerated 1 M HClO₄, in the dark (broken line) and during illumination with monochromatic light, $\lambda = 750$ nm, power ≈ 2.5 mW cm⁻² (full line). Sweep rate 20 mV s⁻¹.

trated by the SEM picture of Fig. 6, top, and by the relevant EDX analysis of Fig. 6, bottom. Prior to electrochemical treatment the electrode composition was close to CuInS₂, except for an area on the right, brighter in the micrograph, where it was close to CuIn₃S₅. Electrodeposition (3 C cm⁻²) is irregularly distributed over the surface. The dark area on the left corresponds to regions where dissolution has progressed more deeply. The main constituent is elemental sulfur (Fig. 6, bottom), whose deposition on the surface is most probably responsible for photocurrent quenching. Going progressively to the right, we first cross a less corroded region with lower sulfur content and then two regions which appear very little corroded and show compositions close to CuInS₂ and CuIn₃S₅. Hence: anodic photocurrent causes oxidation of the electrode material with dissolution of the metal ions and deposition of sulfur; copper poor phases appear less prone to

photoelectro-oxidation, which is consistent with previous findings that they have small (anodic) or inverted (cathodic) photoeffects[14].

To compare the observed phenomena with thermodynamic forecasts, the free energies of formation of the most important species (taken from[15, 16]) are listed in Table 1 and used to estimate the standard potentials of the oxidation reactions reported in Table 2. The values calculated for the case of indifferent (non-protecting) electrolytes show that reactions 1 and 2, forming copper chalcogenides, require the lowest potentials. Reactions 3 and 4, leading to dissolved metal ions, are easier than indicated by standard potentials, due to the low activity of the products; the same applies to reactions 7 and 8, but the latter may be expected to be kinetically limited, due to the number of reactants and more complicated reaction route. Hence, the available experimental evidence appears consistent with thermodynamic and kinetic considerations: (i) the predominant processes are those leading to dissolution of metal ions and sulfur deposition (reactions 1–4), similar to observations reported for photocorrosion of CuIn₅S₈ in a non-protecting electrolyte[17]; (ii) copper sulfides may form in significant amounts (reactions 1 and 2); (iii) some formation of oxidized, soluble sulfur species (reactions 7 and 8) appears likely considering the slow decay of the photocurrent in the experiments under monochromatic light. However, on application of a large (photo)current density, a substantial amount of sulfur originating from reactions 1–5 is deposited on the surface, causing the observed photocurrent quenching.

Current/voltage curves in acidic polyiodide solution

Figure 7 shows a typical dynamic current/voltage curve recorded at *n*-CuInS₂ immersed in the polyiodide solution, under chopped white light. The flatband potential in this medium is $U_{FB} \cong -0.77 \pm 0.05$ V[8]. Negative to the flatband, a small inverted photocurrent is observed, probably associ-

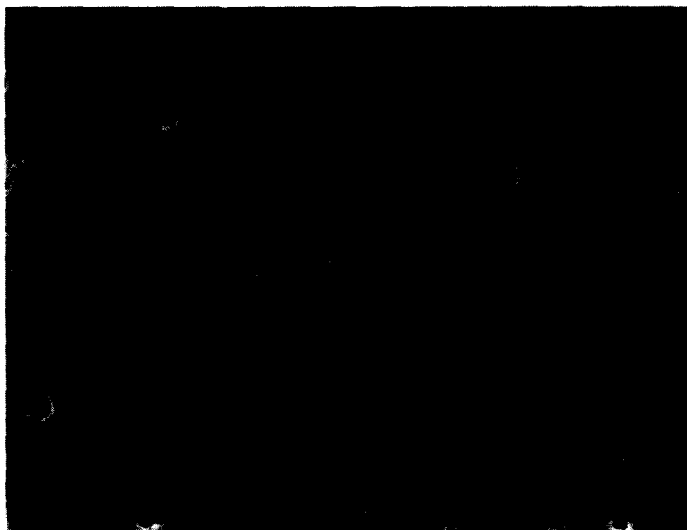


Fig. 4. SEM micrographs of electrode surface after photoelectro-oxidation in 1 M HClO₄ with passage of 30 mC cm⁻².

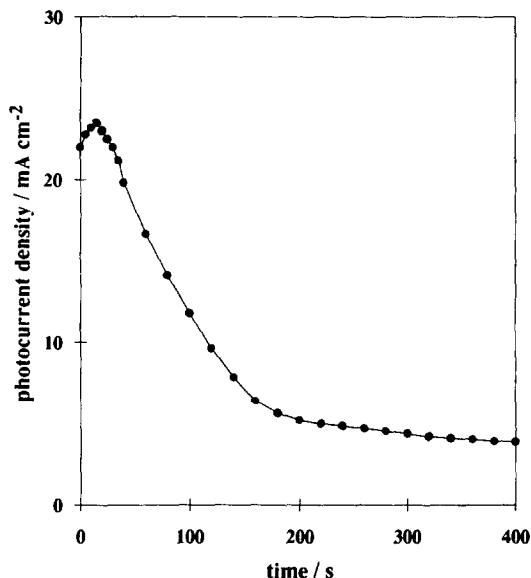


Fig. 5. Typical current/time curve recorded polarizing electrode at 0.4 V in HClO_4 , under white light.

ated with photoconductivity effects in the crystal bulk[14]. Positive to the flatband we observe the onset of anodic photocurrent, which approaches a saturation value when the potential is swept positive of about -0.3 V. The maximum cell output corresponds to a photopotential of about -0.50 V vs. polyiodide[8], namely about -0.40 V vs. *sce*. The fact that electrode photocorrosion in an inert electrolyte becomes significant only at potentials positive of about 0.0 V (Fig. 3), and the consideration that a redox couple with fast electron transfer like polyiodide may provide "kinetic" protection of the semiconductor even in conditions in which the latter would photocorrode[2], ensure that (photo)corrosion provides little contribution to the I-V properties of the photocell in all conditions of practical interest.

Table 1. Gibbs free energy of formation of some species involved in oxidative photodecomposition of CuInS_2 in aqueous acidic solutions (in kJ mol^{-1})

Compound	State	$\Delta G_f^\circ(298)$	Ref.*
CuInS_2	cr	-218.6	15
Cu^+	ao	50.0	16
Cu^{++}	ao	65.5	16
Cu_2S	cr	-86.2	16
CuS	cr	-53.6	16
CuI	cr	-69.5	16
In^{3+}	ao	-98.0	16
In_2S_3	cr	-412.5	16
InI_3	cr	-228	15
I^-	ao	-51.6	16
I_3^-	ao	-51.4	16
H_2O	l	-237.0	16
HSO_3^-	ao	-527.7	16
H^+	ao	0.0	16

* ΔG_f° mostly taken from NBS compilation (Ref. [16]). Standard conditions in all cases 298.15 K and 1 bar. Standard states (second column) correspond to: (cr) solid phase thermodynamically stable in those conditions; (l) aqueous solvent at unit mole fraction; (ao) ion species, not further dissociated, at unity molality in an ideal solution.

(Photo)corrosion in polyiodide solution. Ageing effects

The stability of cell performance during middle term operation was tested in conditions simulating those of a solar cell. Electrodes with a homogeneous CuInS_2 composition (as evaluated by EDX) and almost pure n-type behaviour were investigated. The electrodes, immersed in the polyiodide solution, were illuminated during the day at the applied potential $E = -0.40$ V vs. *sce* and were left overnight in the dark in open circuit conditions. The cell was kept in contact with the atmosphere. Light power was adjusted so as to obtain a photocurrent density of about 40 mA cm^{-2} and the current was monitored for about one week (five-six days of operation) for each electrode. As shown in Fig. 8, the output current decreases, significantly in two cases, and less so in two others.

Table 2. Some oxidative photodecomposition reactions of CuInS_2 in aqueous acidic solutions

Reaction	E_D^0 (vs. <i>nhe</i>)*
<i>a. in indifferent electrolyte</i>	
1. $\text{CuInS}_2 + 3\text{h}^+ \rightarrow \text{CuS} + \text{In}^{3+} + \text{S}$	0.23 V
2. $\text{CuInS}_2 + 3\text{h}^+ \rightarrow \frac{1}{2}\text{Cu}_2\text{S} + \text{In}^{3+} + \frac{3}{2}\text{S}$	0.27 V
3. $\text{CuInS}_2 + 5\text{h}^+ \rightarrow \text{Cu}^{++} + \text{In}^{3+} + 2\text{S}$	0.39 V
4. $\text{CuInS}_2 + 4\text{h}^+ \rightarrow \text{Cu}^+ + \text{In}^{3+} + 2\text{S}$	0.44 V
5. $\text{CuInS}_2 + 2\text{h}^+ \rightarrow \text{Cu}^{++} + \frac{1}{2}\text{In}_2\text{S}_3 + \frac{1}{2}\text{S}$	0.40 V
6. $\text{CuInS}_2 + \text{h}^+ \rightarrow \text{Cu}^+ + \frac{1}{2}\text{In}_2\text{S}_3 + \frac{1}{2}\text{S}$	0.64 V
7. $\text{CuInS}_2 + 3\text{H}_2\text{O} + 9\text{h}^+ \rightarrow \text{Cu}^{++} + \text{In}^{3+} + \text{S} + \text{HSO}_3^- + 5\text{H}^+$	0.42 V
8. $\text{CuInS}_2 + 6\text{H}_2\text{O} + 13\text{h}^+ \rightarrow \text{Cu}^{++} + \text{In}^{3+} + 2\text{HSO}_3^- + 10\text{H}^+$	0.44 V
<i>b. in polyiodide medium</i>	
9. $\text{CuInS}_2 + \text{I}^- + 4\text{h}^+ \rightarrow \text{CuI} + \text{In}^{3+} + 2\text{S}$	0.27 V
10. $\text{CuInS}_2 + 4\text{I}^- + 4\text{h}^+ \rightarrow \text{CuI} + \text{InI}_3 + 2\text{S}$	0.33 V
11. $\text{CuInS}_2 + 3\text{I}^- + 3\text{h}^+ \rightarrow \text{CuS} + \text{InI}_3 + \text{S}$	0.32 V
12. $\text{CuInS}_2 + \text{I}^- + \text{h}^+ \rightarrow \text{CuI} + \frac{1}{2}\text{In}_2\text{S}_3 + \frac{1}{2}\text{S}$	-0.06 V
13. $\text{CuInS}_2 + \text{I}^- + \text{I}_3^- + 2\text{h}^+ \rightarrow \text{CuI} + \text{InI}_3 + 2\text{S}$	0.12 V
14. $\text{CuInS}_2 + \text{I}_3^- + \text{h}^+ \rightarrow \text{CuS} + \text{InI}_3 + \text{S}$	-0.12 V

* $E_D^0 = \Delta G_f^\circ/zF$ for reaction as written. Negative values: oxidation process would occur spontaneously if half-cell were connected to a hydrogen electrode (electrochemical scale[1, 2]). ΔG_f° values calculated from data of Table 1.

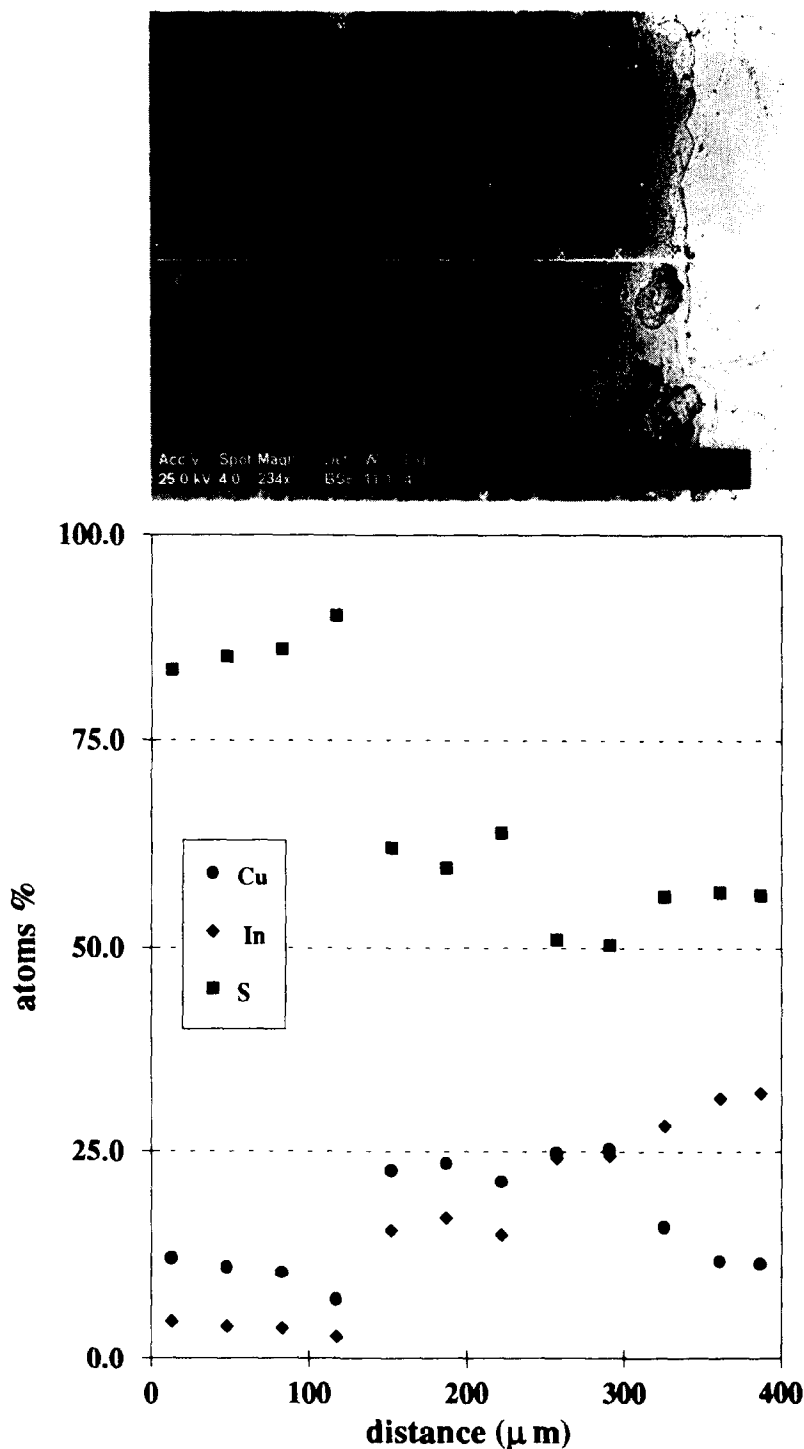


Fig. 6. SEM micrographs of electrode surface (top) after massive photoelectro-oxidation in 1 M HClO₄ (ca. 3.0 C cm⁻²) and relevant EDX composition (bottom). Prior to treatment, EDX composition was close to CuIn₃S₅ in bright area on right, and CuInS₂ elsewhere.

The electrode surface, homogeneously shiny when freshly prepared, shows dull areas upon ageing in the polyiodide solution. The extent of corrosion varied considerably from sample to sample. At electrodes with a largely corroded surface the dark potential is shifted even 200–300 mV in a negative direction with respect to the equilibrium value of the species in

solution, indicating that the interface processes are dominated by some corrosion reaction; electrodes with little corrosion show correspondingly lower shifts of the dark potential.

The SEM pictures show that the shiny areas are still quite smooth, similar to the electrode surface prior to operation, and dull areas are normally

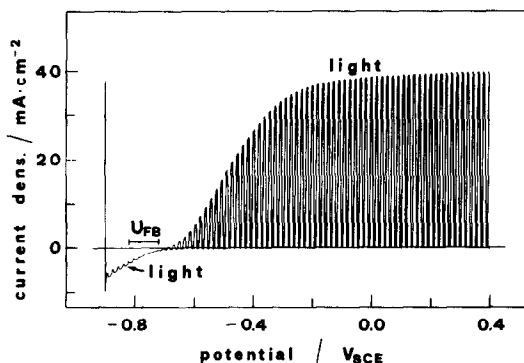


Fig. 7. (Photo)current/voltage curve recorded in polyiodide medium under chopped white light (tungstenhalogen lamp, power on sample about 300 mW cm^{-2}).

stepped (Fig. 9a) and sometimes sponge-like (Fig. 9b). Etching action proceeds with time, since aged electrodes show deeper and more irregular corrosion. EDX microanalyses performed both before and after photoelectrochemical operation show no significant variations in the Cu/In/S ratios and no appreciable iodine signal; also, qualitative analyses performed with a windowless arrangement exclude the significant presence of oxygen.

Hence, SEM-EDX results indicate that corrosion progresses with time but that the composition of the electrode material remains essentially constant—within the sensitivity of the technique. It may be argued that, if any corrosion layer forms, it stays thin by dissolution, the overall process resulting in an approximately stoichiometric removal of constituents from the electrode. Comparison of the decomposition potentials in Table 2a and b show that the polyiodide medium—besides the well known “kinetic” stabilization of the photoelectrode, due to competition for the photogenerated holes—makes electrode decomposition thermodynamically easier. This may be due to the formation of more stable products (metal iodides, compare reactions 9 and 10 with 4, reaction 12 with 6) or to the oxidizing power of the I_3^- species which promotes certain oxidation processes (compare *eg* reaction 13 with 4, reaction 14 with 1). At variance with experiments of (photo)electrodissolution, (photo)corrosion leaves negligible amounts of sulfur on the electrode surface. This is probably because the chalcogen is produced slowly and its accumulation is prevented by oxidation to soluble species by the joint action of photogenerated holes and atmospheric oxygen.

Attempts were made to stabilize the photoanode by adding copper ions to the polyiodide solution, a strategy which proved successful in the case of CuInSe_2 , due to formation of a protective film of $\text{CuISe}_3\text{-Se}^0$ [7, 18]. No marked variation was observed in the cell stability or in the morphology and composition of the corroded surface after this solution modification. Apparently, the formation of a protective film no longer occurs if S replaces Se in the chalcogenide.

The corrosion morphologies of Fig. 9 seem to correspond well to material phases with different compactness, as apparent in the section micrograph of

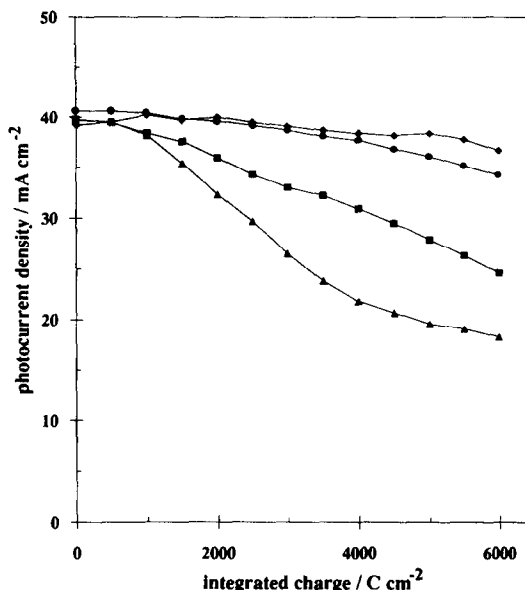


Fig. 8. Photocurrent vs. integrated charge for four $n\text{-CuInS}_2$ photoanodes polarized at -0.4 V in 2.5 M CaI_2 , 2 M HI , 40 mM I_2 under 300 mW cm^{-2} white light.

Fig. 1b. The inner structure of the chalcopyrite layers appears strongly polycrystalline, in contrast with the smooth aspect of the cleavage surface (see pit-free regions of Fig. 4), which seems to be due to a thin surface phase. This fact helps to resolve an apparent inconsistency of earlier structural and spectroscopic investigations[9]: rocking curves, reflecting the conditions of the sample bulk, are quite broad, indicating the existence of a high degree of dislocation or polycrystalline nature; conversely, RHEED, a surface-sensitive technique, shows the pattern of a CuInS_2 surface with good crystalline quality and (112) orientation[9].

CONCLUSIONS

The material, grown under conditions far from equilibrium[9, 10], shows variability in composition, morphology and corrosion behaviour. With reference to the prevailing CuInS_2 phase, corrosion shows the intimate morphology of the layers, which are strongly polycrystalline below a smooth surface. Lamellar CuInS_2 photoanodes may show in an acidic polyiodide solution, satisfactory output stability during middle-term operation. However, significant and irregular corrosion is observed—with quite deep etching in certain spots—which undermines the performance of many photocells. Strategies of interface stabilization based on modifications of the polyiodide solution, which succeeded with CuInSe_2 photoanodes, seem to fail with CuInS_2 . Alternative attempts may involve the use of a more protective electrolyte like polysulfide[15, 17] or photocathodes which are inherently more stable to photodecomposition[1]. The availability of an improved, more homogeneous material is desirable in order to explore these possibilities. Additional

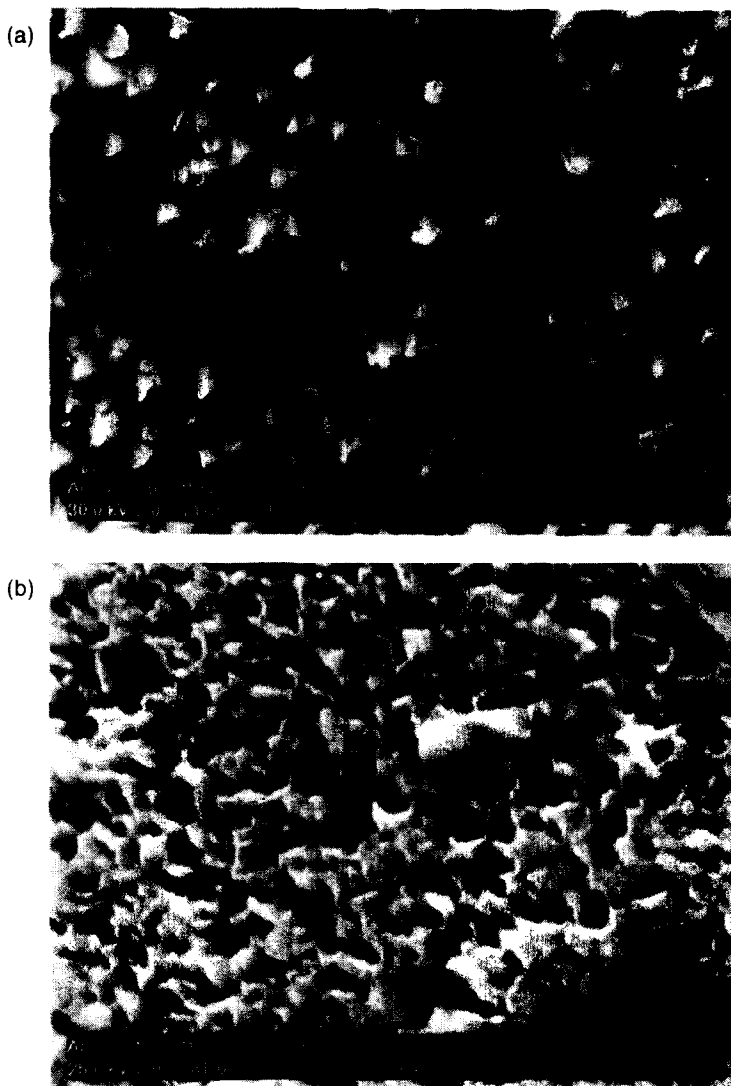


Fig. 9. SEM micrographs of corroded photoanode surface after prolonged operation in polyiodide solution. Note two morphologies, with compact (a) and hollow (b) crystallites, also apparent in side view of Fig. 1b.

effort in the synthesis is in progress and appears justified by the good potential of the layered material[8].

REFERENCES

1. H. Gerischer, *J. electroanal. Chem.* **82**, 133 (1977).
2. H. Gerischer, *J. Vac. Sci. and Technol.* **15**, 1422 (1978).
3. F. Decker, D. A. Soltz and L. Cescato, *Electrochim. Acta* **38**, 95 (1993).
4. P. A. Kohl and D. B. Harris, *Electrochim. Acta* **38**, 101 (1993).
5. G. Razzini, L. Peraldo Bicelli, B. Scrosati and L. Zanotti, *J. electrochem. Soc.* **133**, 351 (1986).
6. D. Cahen and Y. W. Chen, *Appl. Phys. Lett.* **45**, 746 (1984).
7. S. Menezes, H. J. Lewerenz and K. J. Bachmann, *Nature* **305**, 615 (1983).
8. S. Cattarin, N. Dietz and H. J. Lewerenz, *J. electrochem. Soc.* **141**, 1095 (1994).
9. M. L. Fearheiley, N. Dietz and H. J. Lewerenz, *J. electrochem. Soc.* **139**, 512 (1992).
10. S. Fiechter, K. Diesner, N. Dietz, M. Fearheiley, M. Kanis, H.-J. Lewerenz, I. Rechenberg, B. Hermoneit, T. Wirth and W. Kautek, *J. Crystal Growth*, submitted.
11. D. Schmid, M. Ruckh, F. Grunwald and H. W. Schock, *J. appl. Phys.* **73**, 2902 (1993).
12. R. Scheer and H. J. Lewerenz, *J. Vac. Sci. and Technol., A* **12**, 51 (1994).
13. G. Dagan and D. Cahen, *J. electrochem. Soc.* **134**, 592 (1987).
14. S. Cattarin, P. Guerriero, G. Razzini and H. J. Lewerenz, *J. electrochem. Soc.*, **141**, 1100 (1994).
15. D. Cahen and Y. Mirovsky, *J. phys. Chem.* **89**, 2828 (1985).
16. D. D. Wagman, W. H. Evans, V. B. Parker, R. H. Schumm, I. Halow, S. M. Bailey, K. L. Churney and R. L. Nuttall, *J. Phys. Chem. Ref. Data, Suppl.*, **11** (1982).
17. B. Scrosati, L. Fornarini, G. Razzini and L. Peraldo Bicelli, *J. electrochem. Soc.* **132**, 593 (1985).
18. H. J. Lewerenz and E. R. Kötzt, *J. appl. Phys.* **60**, 1430 (1986).